RSC Advances

Cite this: *RSC Advances*, 2012, **2**, 1088–1095

www.rsc.org/advances

PAPER

Adsorption of Hg^{2+} from aqueous solution on functionalized MCM-41

Zhen Zhu, Xinxin Yang, Liang-Nian He and Wei Li*

Received 14th September 2011, Accepted 21st October 2011
DOI: 10.1039/c1ra00720c

Mesoporous MCM-41 has been functionalized using 3-aminopropyltriethoxysilane (KH550) and 3-(2-aminoethylamino)propyldimethoxymethylsilane (KH602). The adsorption behavior of Hg^{2+} on functionalized MCM-41 was investigated systematically. The adsorption rates were very fast and agreed well with pseudo second-order kinetics. The adsorption isotherms fitted the Langmuir model well. The modified MCM-41 adsorbent functionalized using KH602 (NM2) displayed the greatest mercury adsorption efficiency and residual concentration of Hg^{2+} was able to achieve drinking water standards. The regeneration capacity maintained 99.75% performance when the initial solution concentration was 4 mg L^{-1} (4000 ppb) at the tenth cycle, meeting the safe regulatory discharge standard for the first time. Meanwhile, regeneration by washing only with deionized water to remove residual surface Hg^{2+} can cut down the cost of traditional desorption agents and reduce damage to the structure of the adsorbent. Therefore, the adsorbent NM2 has potential and promising application in the field of water pollution control.

Introduction

Global, social and environmental problems such as water pollution have received great attention. Our aim is to reduce the adverse impacts of pollutants and to easily renew.[1–6] Meanwhile, great efforts have been made in developing chemical technologies that can intrinsically reduce or eliminate the use or generation of hazardous substances during the design, manufacture, and use of chemical products—Green Chemistry.[7–10] Heavy metals, particularly mercury, are important environmental pollutants threatening the health of human populations and natural ecosystems alike. Adsorption is a highly effective, economical and reliable chemical engineering method and it is widely applied because of its flexibility, low energy consumption and low operating costs.[11–12] An inherent disadvantage of these materials is their low loading capacities and relatively small metal ion binding constants. However, to circumvent these limitations and improve metal ion loading capacities, many studies have been devoted to researching new selective adsorbents prepared using active organic functions anchored to the surface of suitable supports.

The recently discovered mesoporous silica[13] has received great interest as a solid support because of its unique large surface area, well-defined pore size and shape and its readily modified surface properties. Some of these new mesoporous materials have been functionalized and employed to eliminate traces of toxic heavy metals from contaminated waters.[14–16] These organo functionalized surfaces are resistant to removal from the surface by organic solvents or water.[17] Claudio Airoldi *et al.* made a detailed investigation in the field of adsorption and separation of heavy metal cations on chemically modified silica gel. MCM-41, the most used member of the M41S family, possesses a high surface area and a large pore volume with highly ordered hexagonally packed cylindrical pores.[18] Most importantly, both the surface chemistry and pore openings can be tailored post-synthesis to meet a given requirement. Several studies on the use of functionalized MCM-41 for the removal of mercury ions from contaminated aqueous streams have been reported.[19] Chemically modified MCM-41 containing a variety of chelating groups on a pendant organic chain can be designed for the adsorption and preconcentration of metal ions from aqueous and non-aqueous solutions. Functional groups such as imidazole,[20] amino,[21] iminodiacetic,[22] and EDTA[23] have been successfully incorporated into the inorganic silica matrix,[24–25]

In this work, we report the synthesis of a novel hybrid mesoporous material based on MCM-41. MCM-41 was synthesized using the hydrothermal method as a starting material for surface modification. 3-Aminopropyltriethoxysilane (KH550) (functionalized MCM-41 denoted as NM1) and 3-(2-aminoethylamino)propyldimethoxymethylsilane (KH602) (functionalized MCM-41 denoted as NM2) were chosen because of the presence of nitrogen donor atoms. The adsorption properties of the modified materials were investigated using a batch method. The effects of various parameters such as contact time, pH and temperature on the removal of Hg^{2+} were studied in detail. The sorption equilibrium and kinetics of Hg^{2+} adsorption onto functionalized MCM-41 were studied and the experimental results were described by well-known kinetic and equilibrium equations. Furthermore, the adsorbent NM2 displayed the best mercury adsorption efficiency among all of the adsorbents

Key Laboratory of Advanced Energy Materials Chemistry (Ministry of Education), College of Chemistry, Nankai University, Tianjin, 300071, China. E-mail: weili@nankai.edu.cn; Fax: +86-22-23508662; Tel: +86-22-23508662

tested. This result was attributed to amino groups in the framework of the adsorbents combining with heavy metal ions and improving the adsorption capacity toward heavy metal ions. The adsorption capacity of mercury was sufficient to reduce the residual concentration of Hg^{2+} to drinking water standards. Adsorption cycles were repeated ten times using the same NM2 adsorbent and the residual concentration of Hg^{2+} in the solution remained under 10 ppb when the initial solution concentration was 4 mg L^{-1} (4000 ppb). Compared with the acid regeneration method,[26–28] regeneration by washing only with deionized water to remove residual surface Hg^{2+} can cut down the cost of traditional desorption agents, such as hydrochloric acid, and reduce damage to the structure of the adsorbent so as to prolong the adsorbent life cycle.

Experimental

Materials

N-Cetyl-*N*,*N*,*N*-trimethylammonium bromide (CTAB; 99%) and tetraethoxysilane (TEOS) were bought from Tianjin Chemist Scientific Ltd, China. Mercury(II) chloride, ethanol (EtOH), KH550 (3-aminopropyltriethoxysilane), KH602 (3-(2-aminoethylamino)propyldimethoxymethylsilane), hydrochloric acid (HCl) and activated carbon (coconut-made charcoal) were purchased from Tianjin Jiangtian Chemical Technology Ltd, China. All reagents used in this study were analytical reagent grade.

Synthesis of adsorbents

Mesoporous MCM-41 was crystallized by a hydrothermal method as previously reported.[29] MCM-41 was dispersed in ethanol to which KH550 (40 wt%) was added, and the mixture was refluxed for 6 h at 348 K. The solid material was filtered and cleaned using ethanol, then dried under vacuum at 323 K for 6 h. The amine-grafted MCM-41 was denoted as NM1, indicating the grafting modification method. MCM-41 was dispersed in ethanol to which KH602 (40 wt%) was added, and stirred for 1 h at room temperature (298 K). The solid material was then filtered and cleaned using ethanol, and dried in an oven for 3 h at 393 K. The amine-grafted MCM-41 was denoted as NM2, to indicate the dipping modification method. Meanwhile, to compare the two different modified methods, MCM-41 functionalized using KH550 *via* the dipping method was denoted as NM1-0 and MCM-41 functionalized using KH602 *via* the grafting method was denoted as NM2-0.

Characterization

Powder X-ray diffraction spectra were collected using a Bruker D8 focus diffractometer, with Cu-Kα radiation at 40 kV and 40 mA between 0.6° and 8° (2θ) with a step length of 1 s. Nitrogen adsorption–desorption isotherms of samples at 77 K were measured using a BEL-MINI adsorption analyzer. The surface area was calculated using a multipoint Brunauer–Emmett–Teller (BET) model. The pore size distribution was obtained *via* the BJH model using the desorption isotherms, and the total pore volume was estimated at a relative pressure of 0.99, assuming full surface saturation by nitrogen. Infrared spectra were measured on a Nicolet Nexus 870, Fourier transform spectrometer in the frequency range 400–4000 cm^{-1}. Samples were pulverized and dispersed in KBr pellets before recording the spectra. Elemental analysis was obtained (EA, Elementar Vario EL III) to determine their physical and chemical properties.

Batch adsorption experiments

Hg^{2+} adsorption data from aqueous solution were obtained using the immersion method. The stock solution of Hg^{2+} was prepared using distilled water. The experiments were performed in a temperature-controlled water bath shaker for a certain time at a mixing speed of 180 rpm. The effects of contact time, temperature and pH on adsorption data were assessed by changing the adsorption conditions. The initial pH of the solution was adjusted with HCl solution to reach a desirable value (1–6). Finally, regeneration of the adsorbent was also investigated. At the end of the adsorption process, the adsorbent was filtered and washed using distilled water. The residual concentration of Hg^{2+} was then determined using AAS (TAS-990). The percentage removal of Hg^{2+} was calculated according to the following equation:

$$R = \frac{C_0 - C_e}{C_0} \times 100\% \quad (1)$$

The adsorption amount (Q_e) was calculated according to the following equation:

$$Q_e = \frac{V(C_0 - C_e)}{m} \quad (2)$$

where Q_e (mg g^{-1}) represents the adsorption amount, V (L) represents the volume of the Hg^{2+} solution, C_0 (mg L^{-1}) and C_e (mg L^{-1}) represent the initial and equilibrium liquid-phase concentrations of Hg^{2+}, respectively, and m (g) is the mass of absorbent used in the experiments.

Results and discussion

Characterization of the adsorbents

The small-angle X-ray diffraction (XRD) patterns for MCM-41 and functionalized MCM-41 samples are shown in Fig. 1. Hexagonally arranged channels, represented by (100), (110), and (200) reflections, existed in the samples. The reflection intensity

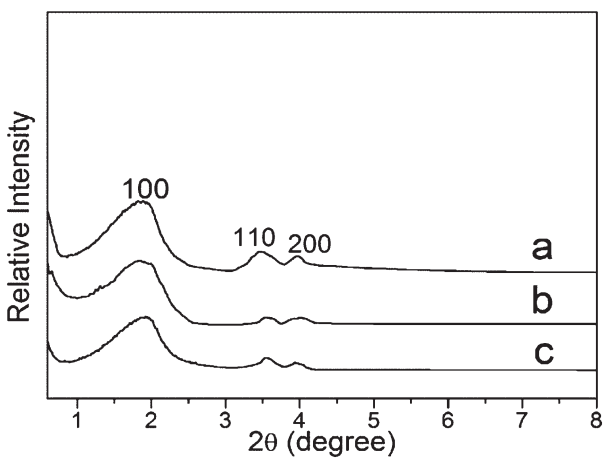

Fig. 1 The small angle XRD patterns of (a) MCM-41, (b) NM1, (c) NM2.

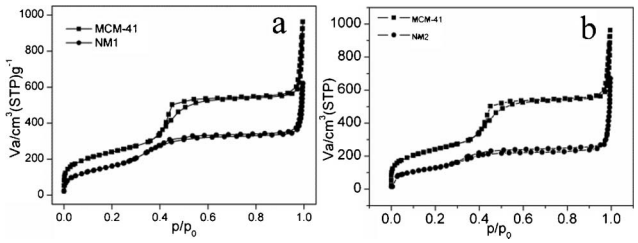

Fig. 2 Nitrogen adsorption/desorption isotherm of modified MCM-41 (a) NM1, (b) NM2.

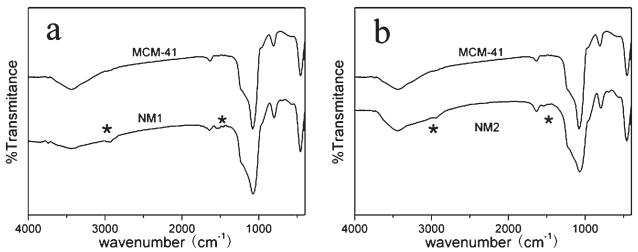

Fig. 3 FT-IR of modified MCM-41 (a) NM1, (b) NM2.

decreased somewhat after functionalization, showing that functional groups have grafted onto the surface of MCM-41, and the porous channels remained in a hexagonal array.

The nitrogen adsorption–desorption isotherms of MCM-41 and chemically modified MCM-41 samples are shown in Fig. 2. They all displayed type IV isotherms with a capillary condensation step, which is characteristic of mesoporous materials according to the classification of the International Union of Pure and Application Chemistry. The porosities calculated from the nitrogen adsorption–desorption data are listed in Table 1. We found that the BET surface area and total pore volume decreased somewhat after functionalization, because of the formation of pendant organic chains, which made the silica gel pore size smaller and some pores even disappeared. These results show that functional groups were successfully loaded onto the MCM-41 surface.

IR spectra of MCM-41 and functionalized MCM-41 between 400 and 4000 cm^{-1} are shown in Fig. 3. MCM-41 includes a large broad band between 3400 and 3200 cm^{-1}, which is attributed to O–H stretching of the surface silanol groups and residual adsorbed water molecules. The intense Si–O–Si stretching vibration band appeared at 1075 cm^{-1}, and the peaks around 882 cm^{-1} and 453 cm^{-1} were attributed to Si–O–Si symmetric stretching and Si–O–Si bending vibrations, respectively. The IR spectra of NM1 and NM2 show that the intensity of the characteristic O–H peak has weakened and the characteristic absorption peak of $–(CH_2)_3–NH_2$ between 2800 and 3000 cm^{-1} indicated that ($–NH_2$) groups have been successfully grafted onto the surface of MCM-41.

Based on all of the above results, we can draw the conclusion that MCM-41 was successfully functionalized and the dipping and grafting methods can successfully graft functional groups on the surface of the MCM-41. Meanwhile, it is possible to calculate the number of molecules attached to the MCM-41 surface from the mass discrepancy between MCM-41 and functionalized MCM-41. As indicated in Table 2, we can conclude that the degree of functionalization obtained in NM1 and NM1-0 were similar. Moreover, the degree of functionalization obtained in NM2 and NM2-0 were also similar. The results revealed that the two independent modified methods have similar effects on modified MCM-41. Compared with the grafting method, which requires 12 h, the dipping method requires only 3 h. Therefore, the dipping method is superior to the grafting method and significantly reduces the cost of the adsorbent.

Table 1 Structural parameters of the samples

Adsorbent	BET surface area ($m^2\ g^{-1}$)	Total pore volume ($cm^3\ g^{-1}$)
MCM-41	834.91	0.920
NM1	648.53	0.715
NM2	508.73	0.681

Adsorption properties for Hg^{2+}

Adsorption performance of different adsorbents. The adsorption performances of MCM-41, NM1, NM2, activated carbon and sulfhydryl resin are shown in Fig. 4. We can see that unfunctionalized MCM-41 exhibited an insignificant adsorption capacity for Hg^{2+} ions and its mercury adsorption capacity is lower than the activated carbon and sulfhydryl resin commercial adsorbents. In contrast, the Hg adsorption capacity shown by the MCM-41 functionalized *via* the grafting route exceeded the capacity of the activated carbon and sulfhydryl resin commercial adsorbents for binding toxic Hg(II) ions from aqueous solutions by a factor of two. This performance is indeed attributed to the ($–NH_2$) groups in the adsorbent that provided the effective adsorption sites. Mercury ions have a preference for coordinating with ($–NH_2$) ligands that have more or less electronegative donor atoms and these have a strong coordination role with Hg^{2+}. In fact, these results are in excellent agreement with the ligand loading values of both NM1 and NM2, as indicated by Fig. 5b. Therefore, the functionalized MCM-41 adsorbent can be well used to remove Hg^{2+} from aqueous solutions. Meanwhile, as indicated in Fig. 5a, when the initial concentration of mercury ions was 4000 ppb, the Hg^{2+} adsorption capacity increased gradually with increasing concentration of modifier solution. Meanwhile, in the case using the same concentrations of different modifiers, the Hg^{2+} adsorption capacity of NM2, which was functionalized using KH602, was better than NM1. In addition, the adsorption capacity of NM2 increased with modifier concentration until the residual concentration of Hg^{2+} under 1 ppb (1 ng mL^{-1}).

These results prove that ($–NH_2$) ligands in the adsorbent are the effective adsorption sites and increasing the number of ligands increases the mercuric ion adsorption capacity of the modified MCM-41. Furthermore, the Hg^{2+} adsorption capacity of NM2 is better than NM1, a result attributed to the presence of two amine positions in the same organic chain reinforcing the mercury adsorption capacity through a cooperative effect related to nitrogen proximity. (Scheme 1 and Scheme 2)

Adsorption kinetics

The adsorption kinetics that described the mercury uptake rate and governed the contact time of the adsorption reaction were one of the important characteristics in defining the efficiency of

Table 2 Physical and chemical properties of the adsorbents

Adsorbent	Loading of functional groups (mmol g^{-1})	Adsorbent	Loading of functional groups (mmol g^{-1})
MCM-41	0	NM2	4.41
NM1	3.17	NM2-0	4.40
NM1-0	3.19		

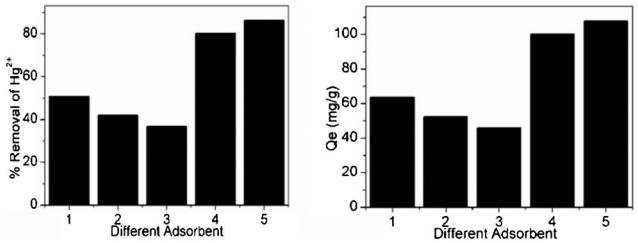

Fig. 4 The adsorption capacity of (1) Activated carbon, (2) Sulfhydryl-resin, (3) MCM-41, (4) NM1 (5) NM2 (adsorption conditions: pH = 6, T = 298 K, contact time = 2 h, initial Hg^{2+} concentration = 250 mg L^{-1}).

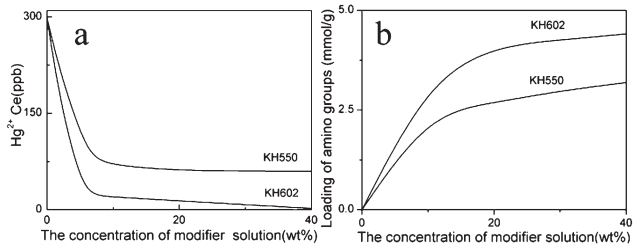

Fig. 5 Effect of different concentration of modifier. (adsorption conditions: initial Hg^{2+} concentration = 4 mg L^{-1} (4000 ppb), contact time = 2 h, pH = 6, T = 298 K).

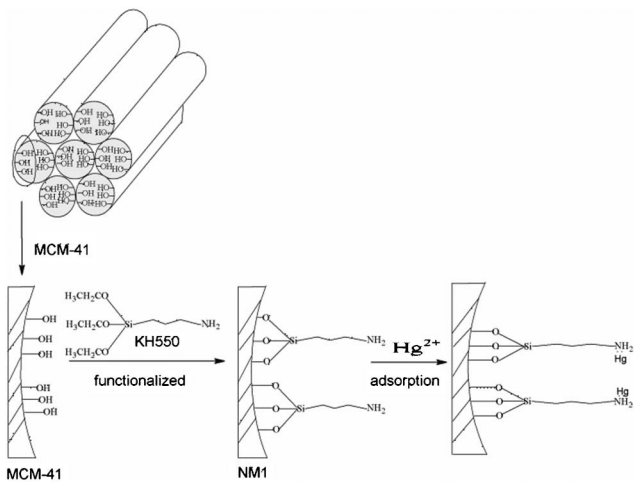

Scheme 1 Schematic mechanism for mercury absorption by NM1.

Hg^{2+} adsorption. Determination of the kinetics of Hg^{2+} adsorption on NM1 was carried out with initial concentrations of 150 mg L^{-1} and 250 mg L^{-1} and on NM2 with initial concentrations of 4 mg L^{-1} and 50 mg L^{-1}, respectively. As illustrated in Fig. 6, the apparent adsorption equilibrium was usually established within 60 min and no significant change was

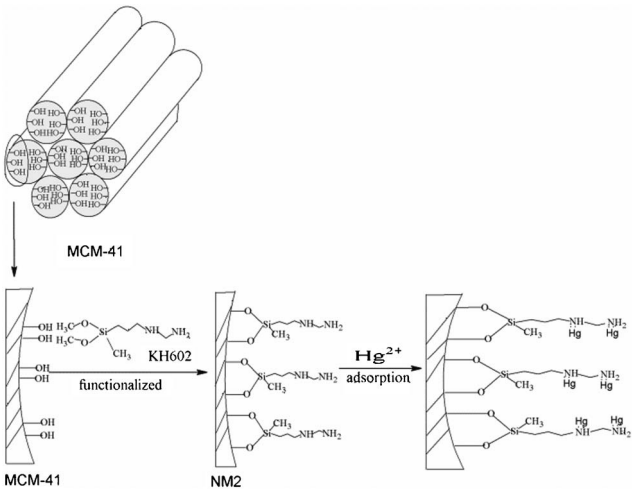

Scheme 2 Schematic mechanism for mercury absorption by NM2.

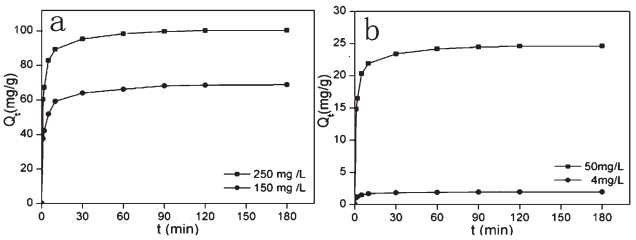

Fig. 6 Kinetic study of Hg^{2+} on functionalized MCM-41 (a) NM1, (b) NM2 (adsorption conditions: adsorbent dose = 2 g L^{-1}, pH = 7, T = 298 K, contact time = 2 h).

observed after 2 h. This was because of the high complexation rate between Hg^{2+} ions and reactive functional groups on the surface of MCM-41. For the physical adsorption process in solution, pseudo first-order and pseudo second-order rate expressions were selected to describe and analyze the adsorption kinetics:

Pseudo first-order rate expression:

$$\ln(Q_0 - Q_t) = \ln Q_0 - k_1 t \quad (3)$$

Pseudo second-order rate expression:

$$\frac{t}{Q_t} = \frac{1}{k_2 Q_0^2} + \frac{1}{Q_0} t \quad (4)$$

Q_0 is the equilibrium adsorption capacity (mg g^{-1}), Q_t is the adsorption capacity over time, k_1 is the pseudo first-order rate constant (min^{-1}), k_2 is the pseudo second-order rate constant

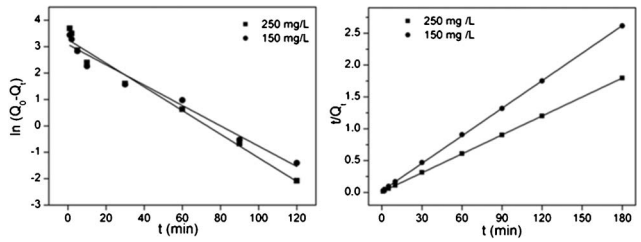

Fig. 7 Pseudo first-order and pseudo second-order kinetic plots for the adsorption of Hg^{2+} on NM1.

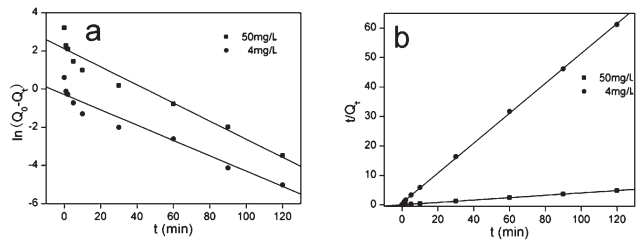

Fig. 8 Pseudo first-order and pseudo second-order kinetic plots for the adsorption of Hg^{2+} on NM2.

(g (mg min)$^{-1}$). As shown in Fig. 7 and Fig. 8, linear relationships were better developed for both NM1 and NM2 using the pseudo second-order rate expression. The values of different parameters determined from pseudo second-order and pseudo first-order kinetic models for Hg^{2+} and their corresponding correlation coefficients are presented in Table 3 and Table 4. The linear correlation coefficient obtained from the pseudo first-order model was not very good, and the calculated equilibrium adsorption capacity Q_{01} (cal) differed from the actual value, indicating that the adsorption is not a pseudo first-order kinetics. It is also clear from Fig. 7a and Fig. 8a that the pseudo first-order model is not suitable to describe the kinetic profile because of the apparent lack of linear behavior. Conversely, rates of aqueous Hg(II) adsorption over amine-grafted MCM-41 material were accurately described by the pseudo second-order equation, as shown in Fig. 7b and Fig. 8b, where experimental t/Q_t and t data are provided, along with linear correlations for the two sets of experiments. The linear correlation coefficient, R^2, was 0.999 and the calculated equilibrium adsorption capacity Q_{02} (cal) was very close to the actual Q_0 (exp), showing that this model is better in explaining the adsorption kinetics of Hg^{2+} on NM1 and NM2.

Adsorption isotherms

The adsorption isotherms of Hg^{2+} on NM1 and NM2 were studied at different temperatures (298, 308, and 318 K) to investigate the effect of temperature. As shown in Fig. 9, all of the adsorption isotherms were nonlinear with curves concave to the abscissa. Each adsorption isotherm initially exhibits a very steep increase, which indicates high-energy adsorption sites favoring strong adsorption at low equilibrium concentrations.

To describe the adsorption isotherm more scientifically, the Langmuir and Freundlich model equations were selected for use in this study. The Langmuir adsorption isotherm has been successfully applied to many pollutant adsorption processes from aqueous solution. It is commonly represented as:

$$Q_e = \frac{Q_0 K_L C_e}{1 + K_L C_e} \quad (5)$$

where Q_e represents the equilibrium adsorption capacity of Hg^{2+} on the adsorbent (mg g^{-1}), C_e represents the equilibrium concentration in solution (mg L^{-1}), Q_0 represents the maximum monolayer capacity of adsorbent (mg g^{-1}), and K_L represents the Langmuir adsorption constant (L mg^{-1}) related to the free energy of adsorption. The Freundlich isotherm is an empirical equation describing adsorption onto a heterogeneous surface. The common form is:

$$Q_e = K_F C_e^{1/n} \quad (6)$$

where K_F (mg g^{-1} (L mg^{-1})$^{1/n}$) and $1/n$ represent the Freundlich constants corresponding to adsorption capacity and adsorption intensity, respectively. The Langmuir and Freundlich model parameters and linear regression correlations obtained from curve fitting are given in Table 5 and Table 6. It can be seen that linear regression correlations using the Langmuir model were better than those for the Freundlich isotherm for mercury ions, which suggests that the Langmuir model better describes the adsorption of Hg^{2+} on NM1. These results indicate that the adsorption is of a typical monomolecular-layer form. Moreover, the values for $1/n$ from the Freundlich model were all less than 1, which is indicative of high adsorption intensity between Hg^{2+} and the adsorbent.

Table 3 Fitting parameters for Hg^{2+} adsorption on NM1

		Pseudo first-order			Pseudo second-order		
C_0 (mg L^{-1})	Q_0(exp) (mg g^{-1})	Q_{01}(cal) (mg g^{-1})	k_1 (min^{-1})	R^2	Q_{02}(cal) (mg g^{-1})	k_2 (g(mg min)$^{-1}$)	R^2
150	68.82	68.14	0.039	0.967	69.32	0.018	0.999
250	100.25	98.13	0.045	0.974	101.11	0.017	0.999

Table 4 Fitting parameters for Hg^{2+} adsorption on NM2

		Pseudo first-order			Pseudo second-order		
C_0 (mg L^{-1})	Q_0(exp) (mg g^{-1})	Q_{01}(cal) (mg g^{-1})	k_1 (min^{-1})	R^2	Q_{02}(cal) (mg g^{-1})	k_2 (g(mg min)$^{-1}$)	R^2
50	24.64	24.31	0.055	0.962	24.78	0.346	0.999
4	1.98	1.96	0.049	0.961	1.99	0.339	0.999

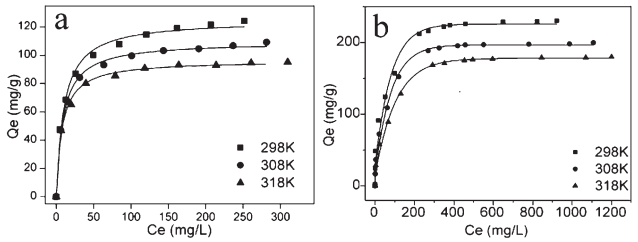

Fig. 9 Adsorption isotherm of Hg^{2+} on functionalized MCM-41 at different temperatures (a) NM1, (b) NM2 (adsorption conditions: adsorbent dose = 2 g L^{-1}, contact time = 2 h, pH = 6).

Table 5 Parameters of adsorption model at different temperatures (NM1)

T/K	Langmuir model			Freundlich model		
	Q_0 (mg g^{-1})	K_L (L mg^{-1})	R^2	K_F [mg g^{-1} (L $mg^{-1})^{1/n}$]	$1/n$	R^2
298	125.06	0.147	0.981	41.569	0.206	0.954
308	109.70	0.125	0.996	41.813	0.178	0.928
318	96.44	0.098	0.995	41.572	0.153	0.910

Table 6 Parameters of adsorption model at different temperatures (NM2)

	Langmuir model			Freundlich model		
T/K	Q_0 (mg g^{-1})	K_L (L mg^{-1})	R^2	K_F [mg g^{-1} (L $mg^{-1})^{1/n}$]	$1/n$	R^2
298	231.92	0.131	0.982	36.941	0.210	0.956
308	201.40	0.106	0.991	35.406	0.169	0.927
318	182.73	0.088	0.993	37.380	0.147	0.905

The monolayer capacity Q_0 of Hg^{2+} on NM1 at 298 K (125.06 mg g^{-1}), 308 K (109.70 mg g^{-1}) and 318 K (96.44 mg g^{-1}), respectively, was calculated based on the Langmuir isotherm. The monolayer capacity Q_0 of Hg^{2+} on NM2 at 298 K (231.92 mg g^{-1}), 308 K (201.40 mg g^{-1}) and 318 K (182.73 mg g^{-1}), respectively, was also calculated based on the Langmuir isotherm (Fig. 9). As expected, the maximum adsorptive capacity decreased with increasing temperature, indicating that the adsorption process was exothermic (Table 7 and Table 8).

It is worth noting that the adsorption capacity of NM2 for Hg(II) is higher than that of NM1. The reason is that the KH602 organic chain has two amino groups and the KH550 organic chain has only one amino group, amino groups in the adsorbent are the effective adsorption sites.

Thermodynamic studies

Using the following equations, the thermodynamic parameters of the adsorption process were determined from the experimental data:

Table 7 Thermodynamic data for adsorption of Hg^{2+} on NM1

T/K	K_L (L mol^{-1})	ΔH (kJ mol^{-1})	ΔS (J $mol^{-1}K^{-1}$)	ΔG (kJ mol^{-1})
298	29567	−15.96	32.16	−25.51
308	25134	−15.96	32.16	−25.95
318	19698	−15.96	32.16	−26.14

Table 8 Thermodynamic data for adsorption of Hg^{2+} on NM2

T/K	K_L (L mol^{-1})	ΔH (kJ mol^{-1})	ΔS (J $mol^{-1}K^{-1}$)	ΔG (kJ mol^{-1})
298	26291	−15.62	32.16	−25.20
308	21308	−15.62	32.16	−25.51
318	17714	−15.62	32.16	−25.85

Van't Hoff equation:

$$\ln\frac{Q_e}{C_e} = \frac{-\Delta H}{RT} + C \quad (7)$$

Gibbs free energy equation:

$$\Delta G = -RT\ln K_L \quad (8)$$

where K_L is the distribution coefficient for the adsorption; ΔS, ΔH and ΔG are the changes of entropy, enthalpy and the Gibbs energy, respectively; T/K is the temperature; R (J mol^{-1} K^{-1}) the gas constant, Q_e is the equilibrium adsorbate concentration in the aqueous phase (mg g^{-1}) and C_e is the equilibrium concentration in solution (mg L^{-1}), The values of ΔH and ΔS were determined from the slopes and intercepts of the plots of $\ln K_L$ *versus* $1/T$ (as illustrated in Fig. 10), when measured under the same experimental conditions. As expected the maximum adsorptive capacity decreased with the increase of temperature, indicating that the adsorption process was exothermic (Table 7 and Table 8).

Effect of pH values on Hg^{2+} adsorption

In practical industrial processes, wastewater may be acidic or alkali and may contain many other contaminants besides mercury. The pH of a solution is one of the most important parameters in the adsorption process. To investigate the effect of pH on the adsorption performance of Hg^{2+}, aqueous solutions were prepared with different pH values ranging from 1 to 6. As illustrated in Fig. 11, the pH value obviously had a considerable influence on the adsorption capacities of both NM1 and NM2. The adsorption capacity was highest at pH 6, and the adsorption capacity for Hg^{2+} ions clearly decreased with decreasing pH. The significant impact of solution pH on Hg(II) uptake could be explained by changes in both the amidogen in the adsorbents and aqueous Hg(II) speciation. In acidic solution, Hg^{2+} is usually the dominant species. Compared with relatively small hydrated species, such as $Hg(OH)^+$ and $Hg(OH)_2$, Hg^{2+} has lower affinity with nitrogen-containing binding sites, causing a decrease in mercury adsorption capacity. In addition, at low pH values, the concentration of H^+ at the surface was much higher. The large

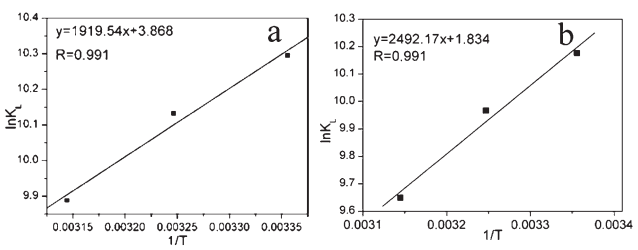

Fig. 10 Plot of $\ln K_L$ *vs.* $(1/T)$ (a) NM1, (b) NM2.

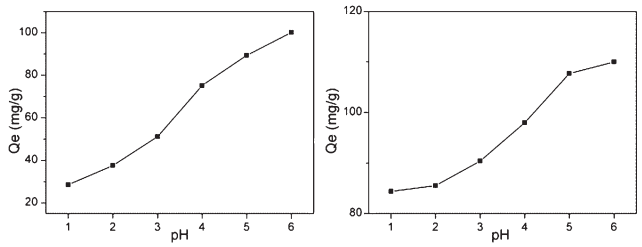

Fig. 11 Effect of pH on the adsorption of Hg^{2+} onto functionalized MCM-41 (a) NM1, (b) NM2 (adsorption conditions: initial Hg^{2+} concentration = 250 mg L^{-1}, adsorbent dose = 2 g L^{-1}, contact time = 2 h, pH = 6, T = 298 K).

amount of H^+ repelled the positively charged Hg^{2+} as a result of the electrostatic potential and prevented Hg^{2+} adsorbing onto the surface of the grafted MCM-41 so that the adsorption capacity was lower. With increasing pH, the concentration of H^+ decreased, and the electrostatic repulsion decreased sharply, allowing a greater quantity to be adsorbed.

Regeneration

The cost of adsorbents is one of the most important factors in the adsorption industry. Therefore, the regeneration properties of NM2 were studied. The choice of eluents is important for recovery and regeneration of the MCM-41 adsorbents. We designed a new regeneration method denoted as water regeneration method, which is based only on deionized water, thus minimizing the use of corrosive acids, along with chemicals that react with or form strong complexes with the grafted functional groups. This water regeneration method was as follows: the sorbed Hg^{2+}-loaded samples were placed in deionized water, stirred for 3 h, centrifuged at 8000 rpm for 10 min at 323 K, then filtered with deionized water, and the Hg^{2+} completely desorbed. The acid regeneration method was as follows: the sorbed Hg^{2+}-loaded samples were washed twice with distilled water to remove residual Hg^{2+} on the surface, then placed in 0.1 mol L^{-1} HCl solution, stirred for 3 h, and centrifuged at 8000 rpm for 10 min, after which the Hg^{2+} completely desorbed. The two different regeneration methods were compared, as indicated in Fig. 12. After acid regeneration, the adsorption capacity of NM2 for Hg^{2+} decreased, and the degree of loss accelerated with increasing regeneration time. After the tenth regeneration, 91% of the adsorption capacity still remained. The reason may be that hydrochloric acid can react with amino groups of NM2, the

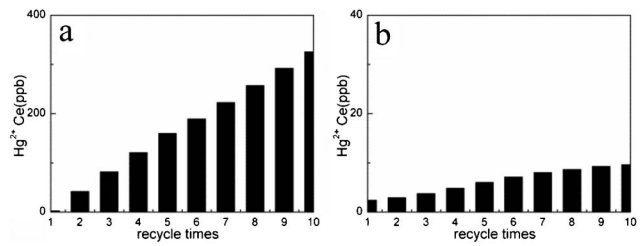

Fig. 12 Regenerated use of NM2 adsorbent for the removal of Hg^{2+} (a) acid regeneration method (b) water regeneration method (adsorption conditions: initial Hg^{2+} concentration = 4 mg L^{-1} (4000 ppb), contact time = 2 h, pH = 6, T = 298 K).

number of amino groups has decreased, and some adsorption sites have deactivated. Compared with the hydrochloric acid regeneration method for NM2, an interesting feature of the NM2 regeneration *via* our water regeneration method is that for an initial concentration of Hg^{2+} ions of 4000 ppb (4 mg L^{-1}), 99.75% of the adsorption capacity of recycled NM2 can still be maintained and a residual concentration of Hg^{2+} under 10 ppb (10 ng mL^{-1}) could be obtained at the tenth cycle. This result may be explained by the adsorption process being exothermic, so that the desorptive capacity increased with increasing temperature. At the same time, the amino groups of NM2 have a coordination role with mercury ions and the number of amino groups has decreased slightly because the water regeneration method includes only deionized water instead of hydrochloric acid solution. Compared with the acid regeneration method, this water regeneration method can cut down the cost of desorption agents such as hydrochloric acid and reduce the extent of structural damage to the adsorbents, thus prolonging the life of the adsorbent. This fact could probably be associated with steric hindrance due to the increase in the number of pendant chains on the MCM-41 surface, the results obtained with mercury cations showed a decrease in binding on the MCM-41 surface (moderate intermolecular force), mercury ions could easily desorb under mild conditions without using desorption agents. Consequently, it could be concluded that NM2 could be used more economically in an actual process to remove trace mercury from water to meet regulatory safe discharge standards.

Conclusions

Mesoporous MCM-41 amine-functionalized with organic chains containing one, two amino functional groups have been successfully synthesized by dipping and grafting to achieve mercury(II) adsorbents from aqueous solution. Compared with the grafting method, the dipping method requires less time to perform. Therefore, the dipping method is superior to the grafting method and significantly reduces the cost of the adsorbent. The adsorption kinetics for Hg^{2+} showed that the adsorption rates on NM1 and NM2 were very fast and in good agreement with pseudo second-order kinetics. The adsorption isotherm fitted the Langmuir model well and the maximum adsorption capacity of NM2 was 231.92 mg g^{-1}. The higher adsorption capacity of NM2 compared with MP-MCM-41[30] 118.35 mg g^{-1}, unfunctionalized MCM-41, NM1, activated carbon and sulfhydryl resin commercial adsorbents may be attributed to the ability of Hg^{2+} to form covalent bonds with the ($-NH_2$) and (–SH) groups to coordinate heavy metal ions. This causes a significant enhancement of the capacity toward heavy metal ions. Furthermore, the presence of two amino positions in the same organic chain enhances the mercury(II) adsorption capacity and amino groups have better adsorption capacity for Hg^{2+} ions than (–SH) groups. The pH values had a major impact on Hg^{2+} adsorption. NM2 can be regenerated efficiently, which will enable them to be used for at least ten cycles without significant change in adsorption capacity when the initial concentration of Hg^{2+} is 4000 ppb. Regeneration of the mercury-loaded adsorbent was achieved under mild conditions by washing with only deionized water. The sample NM2 shows potential for application as an effective and economical adsorbent for the removal of low

concentrations of Hg(II) from aqueous solutions, such as contaminated industrial effluents.

Acknowledgements

The authors acknowledge financial support from the National Natural Science Foundation of China (Grant Nos. 21073098), the Natural Science Foundation of Tianjin (11JCZDJC21600), and the Research Fund for MOE (IRT-0927), the Doctoral Program of Higher Education (20090031110015), and the Program for New Century Excellent Talents in University (NCET-10-0481).

References

1 Z.-Z. Yang, Y.-N. Li, Y.-Y. Wei and L.-N. He, *Green Chem.*, 2011, **13**, 2351.
2 C.-X. Miao, B. Yu and L.-N. He, *Green Chem.*, 2011, **13**, 541.
3 Z.-J. Wang, Y. Zhao, L. Cui, H.-Y. Du, P. Yao and C.-J. Liu, *Green Chem.*, 2007, **9**, 554.
4 W. L. IJdo and T. J. Pinnavaia, *Green Chem.*, 2001, **3**, 10.
5 S. Zhang and Z. C. Zhang, *Green Chem.*, 2002, **4**, 376.
6 M. Nefedieva, O. Lebedeva, S. Borisenkova, D. Kultin, L. Kustov and V. Krasovskiy, *Green Chem.*, 2010, **12**, 346.
7 R. Skouta, R. S. Varma and C.-J. Li, *Green Chem.*, 2005, **7**, 571.
8 C.-J. Li, *Acc. Chem. Res.*, 2004, **43**(4), 581.
9 M. Selva, P. Tundo, D. Brunelli and A. Perosa, *Green Chem.*, 2007, **9**, 463.
10 T. Pietro and P. Alvise, *Chem. Soc. Rev.*, 2007, **36**(3), 532.
11 W.-J. Choi, K.-C. Cho, S.-S. Lee, J.-G. Shim, H.-R. Hwang, S.-W. Parkd and K.-J. Oh, *Green Chem.*, 2007, **9**, 594.
12 M. Minamisawa, H. Minamisawa, S. Yoshida and N. Takai, *Green Chem.*, 2005, **7**, 595.
13 X.-X. Wang, X.-L. Ma, L. Sun and C.-S. Song, *Green Chem.*, 2007, **9**, 695.
14 H. Yoshitake, T. Yokoi and T. Tatsumi, *Chem. Mater.*, 2003, **15**, 1713.
15 T. Yokoi, T. Tatsumi and H. Yoshitake, *Bull. Chem. Soc. Jpn.*, 2003, **76**, 2225.
16 P.-Q. Damián, I. D. Hierro, M. Fajardo and I. Sierra, *J. Environ. Monit.*, 2006, **8**, 214.
17 A. G. S. Prado, L. N. H. Arakaki and C. Airoldi, *Green Chem.*, 2002, **4**, 42.
18 A. V. Neimark, P. I. Ravikovitch, M. Grün, F. Schüth and K. K. Unger, *J. Colloid Interface Sci.*, 1998, **207**, 159.
19 V. Manu, H. M. Mody, H. C. Bajaj and R. V. Jasra, *Ind. Eng. Chem. Res.*, 2009, **48**, 8954.
20 J. Li, T. Qi, L. Wang, C. Liu and Y. Zhang, *Mater. Lett.*, 2007, **61**, 3197.
21 J. Aguado, J. Arsuaga, A. Arencibia, M. Lindo and V. Gasc, *J. Hazard. Mater.*, 2009, **163**, 213.
22 Z. Gao, L. Wang, T. Qi, J. Chu and Y. Zhang, *Colloids Surf., A*, 2007, **304**, 77.
23 Y. Yang, N. Ma, Q. Zhang and S. Chen, *J. Appl. Polym. Sci.*, 2009, **113**, 3638.
24 V. K. Saini, M. Pinto and J. Pires, *Green Chem.*, 2011, **13**, 1251.
25 A. Bibby and L. Mercier, *Green Chem.*, 2003, **5**, 15.
26 Y. Zhao, Y. Chen, M.-S. Li, S.-Y. Zhou, A. Xue and W.-H. Xing, *J. Hazard. Mater.*, 2009, **171**, 640.
27 R.-J. Qu, Y. Zhang, C.-M. Sun, C.-H. Wang, C.-N. Ji, H. Chen and P. Yin, *J. Chem. Eng.*, 2010, **55**, 1496.
28 V. Antochshuk, O. Olkhovyk, M. Jaroniec, I.-S. Park and R. Ryoo, *Langmuir*, 2003, **19**, 3031.
29 V. Elías, E. Vaschetto, K. Sapag, M. Oliva, S. Casuscelli and G. Eimer, *Catal. Today*, 2011, **172**, 58.
30 L. Mercier and T. J. Pinnavaia, *Environ. Sci. Technol.*, 1998, **32**, 2749.